AIP | Physics of Plasmas

For $q=0.85$ at $t=3000$

Nonlinear Landau damping and formation of Bernstein-Greene-Kruskal structures for plasmas with q-nonextensive velocity distributions

M. Raghunathan and R. Ganesh

Related Articles

Additional information on Phys. Plasmas
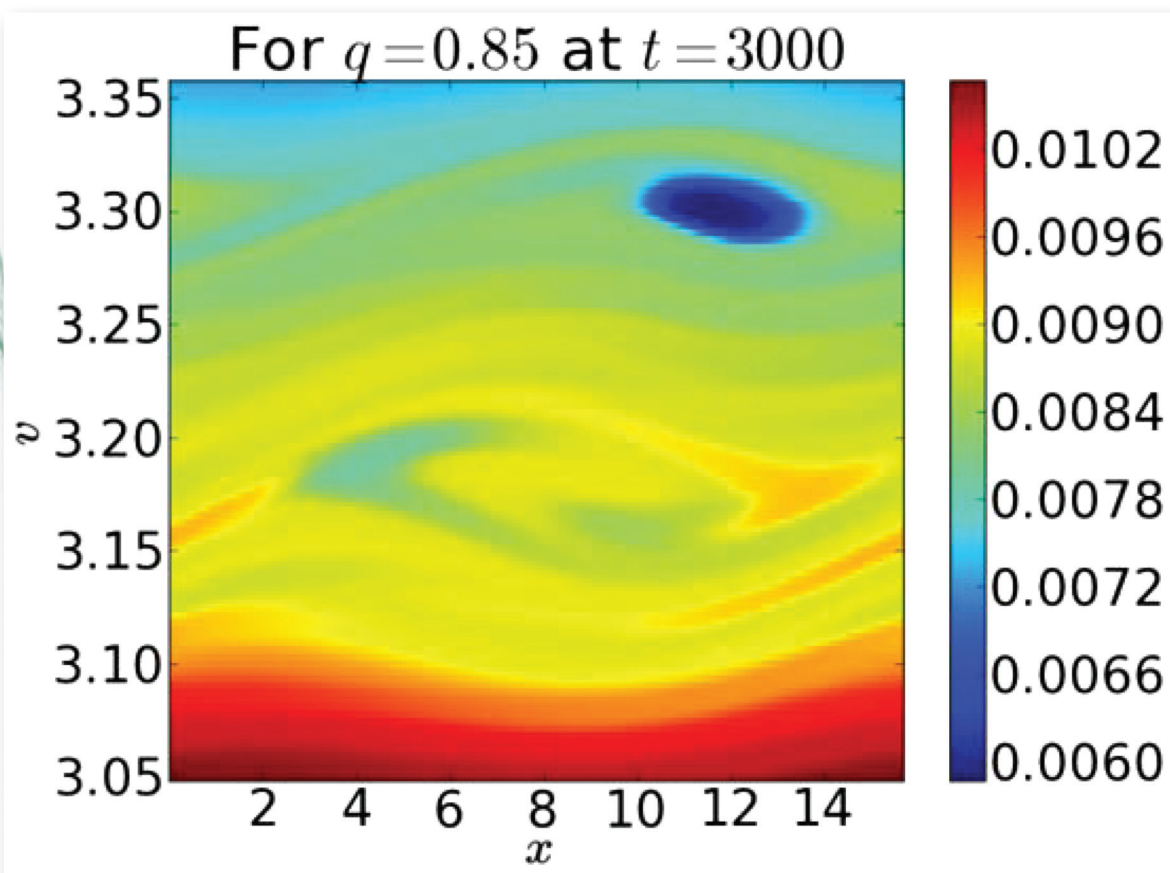
Nonlinear Landau damping and formation of Bernstein-Greene-Kruskal structures for plasmas with *q*-nonextensive velocity distributions

M. Raghunathan[1] and R. Ganesh[2]
[1]*Indian Institute of Science Education and Research (IISER), Pune 411021, India*
[2]*Institute for Plasma Research, Gandhinagar 382428, India*

In the past, long-time evolution of an initial perturbation in collisionless Maxwellian plasma ($q = 1$) has been simulated numerically. The controversy over the nonlinear fate of such electrostatic perturbations was resolved by Manfredi [Phys. Rev. Lett. **79**, 2815–2818 (1997)] using long-time simulations up to $t = 1600\omega_p^{-1}$. The oscillations were found to continue indefinitely leading to Bernstein-Greene-Kruskal (BGK)-like phase-space vortices (from here on referred as "BGK structures"). Using a newly developed, high resolution 1D Vlasov-Poisson solver based on piecewise-parabolic method (PPM) advection scheme, we investigate the nonlinear Landau damping in 1D plasma described by toy q-distributions for long times, up to $t = 3000\omega_p^{-1}$. We show that BGK structures are found only for a certain range of q-values around $q = 1$. Beyond this window, for the generic parameters, no BGK structures were observed. We observe that for values of $q < 1$ where velocity distributions have long tails, strong Landau damping inhibits the formation of BGK structures. On the other hand, for $q > 1$ where distribution has a sharp fall in velocity, the formation of BGK structures is rendered difficult due to high wave number damping imposed by the steep velocity profile, which had not been previously reported. Wherever relevant, we compare our results with past work. © *2013 American Institute of Physics*. [http://dx.doi.org/10.1063/1.4794320]

I. INTRODUCTION

Exponential damping of small vibrations in uniform, one-dimensional, collisionless, Maxwellian, electronic plasma was first pointed out by Landau by correctly accounting for the singularity in the contour integral for the dispersion relation.[1] It meant that damping occurs in a perturbed plasma despite the absence of any dissipative term. Since then, this has been shown in innumerable simulations for collisionless plasmas. As is well known, Landau's treatment is restricted to infinitesimal perturbations, which helps approximate the system to be linear. This helps simplify the system and, from there on, is solved rigorously.

However, as the amplitude of perturbation becomes larger, contribution from the nonlinear terms become more significant, and the behaviour deviates from uniform exponential damping. The approximate analytical solutions available for nonlinear damping are not valid for long-times. For example, O'Neil analytically showed that the system undergoes oscillations with trapping time τ as the period and that the damping rate goes to zero with times much greater than the trapping time.[2] However, O'Neil's treatment is not applicable for times much greater than the trapping time.

For a many decades, the fate of nonlinear finite amplitude electrostatic perturbations for times much greater than O'Neil trapping time was an open problem. The question of whether electrostatic perturbations will damp away at $t \to \infty$ or would lead to the formation of Bernstein-Greene-Kruskal (BGK)[3] structures was hotly debated. For example, in 1997, Isichenko proposed that such perturbations undergo Landau damping following an algebraic decay.[4] However, this

derivation itself was under the assumption of decay of the field. Soon, Manfredi observed from long-time numerical simulations up to $1600\omega_p^{-1}$ that for a finite amplitude perturbations the plasma undergoes a few amplitude oscillations (O'Neil oscillations) and then approaches a steady-state[5] similar to BGK mode. Furthering this debate, in 2000, Firpo and Elskens proposed a Hamiltonian model wherein it was shown that there exists a critical wave-intensity above which Landau damping leads to a finite field amplitude and below which equilibrium amplitude vanishes.[6] Later in 2004, Ivanov *et al.*, using Vlasov simulations, have also found the existence of such a critical perturbation amplitude.[7] Further, in 2009, Barré and Yamaguchi, using a Hamiltonian mean-field model, have shown that systems with repulsive interactions, such as plasmas, can indeed sustain long-lasting small travelling clusters and have discussed the existence of an upper limit on the value of the perturbation amplitude for which trapping occurs.[8]

However, these studies were for Maxwellian plasmas. As is well known, Maxwellians may not adequately describe systems with long-range interactions. It is also well-known that for a system with short range interactions, the energy of the system is additive or extensive. Therefore, maximizing Boltzmann-Gibbs-Shannon (BGS) entropy under energy constraints leads to a Maxwellian. For systems which interact with long-range interactions and for which energy is not additive or extensive, deviations from BGS statistics have been attempted leading to non-extensive generalizations. For example, Tsallis defines a q-nonextensive entropy functional,[9] where q is the strength of nonextensivity, and the corresponding q-distribution is derived as an extremum state of this new entropy functional.[10] The q-distributions lend

20, 032106-1

themselves to applications in vast number of problems in plasmas.[11,12] The q-distribution has also been able account for the velocity distributions of gravitational systems such as galaxy clusters.[13]

The trapping of particles for nonlinear Landau damping in q-distributions has been studied by Valentini in the past.[14] However, these simulations performed were for relatively smaller deviations around $q = 1$, for gridsizes smaller than Manfredi's simulations and for times up to $1200\omega_p^{-1}$. Also, this work[14] is exclusively concerned with the dependence of trapping of particles on perturbation amplitude and the resulting bounce time. In this work, it is argued that the effect of increasing damping rate and bounce time with decreasing value of q limits trapping for $q < 1$ whereas trapping is efficient for $q > 1$. However, to the authors's knowledge, the phenomenon has not been studied for variations of perturbation wavenumber and its effect on limiting the range of q for which such trapping can be found. We explore the presence of BGK structures over a broader range of q around $q = 1$ and determine numerically the extent to which trapping depends on the value of perturbation wavenumber. The simulations undertaken have been run till $3000\omega_p^{-1}$ on gridsizes comparable to Manfredi's simulations. In the case of $q > 1$, we also find that simulations till $1200\omega_p^{-1}$ do not let the numerical entropy settle to a stable value, hence making it necessary to prolong the simulations in order to confirm a numerical steady-state. This, for $q < 1$, brings to our attention a new behaviour of the system. On extending the simulations, we confirm that the increasing damping rate with decreasing q puts a lower limit on q beyond which no trapping occurs. This confirms Valentini's findings for $q < 1$.[14] We find additionally that for $q > 1$, damping is restricted by an upper limit on the perturbation wavenumber k, which in turn imposes an upper limit on the value of q for trapping, which was previously not addressed.

We proceed to describe the mathematical model and the numerical code in Sec. II and the simulations in Sec. III, and we present our conclusions in Sec. IV.

II. THE NUMERICAL CODE

We first construct a numerical solver that can self-consistently solve both the Vlasov and Poisson equations and advance the solution in time. A one-dimensional, collisionless plasma can be modelled using the Vlasov-Poisson system, given by

$$\frac{\partial f}{\partial t} + v\frac{\partial f}{\partial x} + E\frac{\partial f}{\partial v} = 0, \quad \frac{\partial E}{\partial x} = \int f \, dv - 1, \qquad (1)$$

where $f(x, v, t)$ is the electron distribution function and $E(x, t)$ is the electric field. For this system, time has been normalized to the plasma frequency ω_p, space has been normalized to the Debye length λ_D, and velocity has been normalized by $v_{th} = \lambda_D\omega_p$. Consequently, f gets normalized by n_0/v_{th} and E by $-m_e v_{th}^2/e\lambda_D$. In this model, the ions form a stationary neutralizing background of number density n_0. Hence, the numerical value of "1" in the Poisson equation. One can see that any unperturbed normalized velocity

distribution function, in the absence of a background electric field, is a solution of the Vlasov-Poisson system.

In order to solve Eq. (1), we use the time-stepping method suggested by Cheng and Knorr.[15] We apply the following time-stepping for one time step Δt:

- Solve $\partial f/\partial t + v\partial f/\partial x = 0$ for $\Delta t/2$, for a given v in the v-domain.
- Solve the Poisson equation to obtain $E(x)$.
- Solve $\partial f/\partial t + E\partial f/\partial v = 0$ for Δt, for an E in the obtained $E(x)$.
- Again, solve $\partial f/\partial t + v\partial f/\partial x = 0$ for $\Delta t/2$, for a given v in the v-domain.

Thus, the solution of the system is reduced to solving two 1D advection equations and a Poisson equation. This method formally incurs an error of the order $O((\Delta t)^3)$. Further, this requires a reliable advection solver and a Poisson solver. There are several methods of implementing this time-stepping method depending on how one chooses to evolve the advections.[16] We select an Eulerian fixed grid advection scheme for the solution of the advection equation. The advantage of doing so is that the advections are constant speed advections, for which various methods are available. Some of the advection methods are, for example, are flux-balance (FB) method,[16,17] piecewise-parabolic method (PPM),[16,18] and flux-corrected transport (FCT) method.[16,19]

From the conclusions of Arber and Vann,[16] we choose the PPM advection method as our advection solver. The PPM advection method is formally third-order accurate away from the extrema and first-order accurate at the extrema. Also, the monotonicity limiters of the PPM method ensure that the positivity of the distribution function is maintained. However, since the PPM advection method is an explicit method, it is restricted by the Courant-Frederichs-Löwy (CFL) condition. Therefore, we avoid the restriction set forth by the CFL condition by shifting the function by an integral number of grid points (depending on the CFL number) and then apply PPM advection on the remainder of the timestep which satisfies the CFL condition.[16]

We let $0 < x < L$, where L is the system size in x, and $-v_{max} < v < v_{max}$, where v_{max} is chosen sufficiently large so that the velocity distribution function approaches zero as $|v|$ approaches v_{max}. We apply periodic boundary conditions (PBC) along both boundaries for x and v. The unphysical effects of the PBC on the velocity grid are mitigated by choosing a sufficiently large value of v_{max}. The grid spacing is given by $\Delta x = L/N_x$ and $\Delta v = 2v_{max}/N_v$.

Also, we use a Fourier transform based method to solve the Poisson equation. To the Poisson equation

$$\frac{\partial E(x)}{\partial x} = \rho(x), \qquad (2)$$

we apply Fourier transform and get

$$ik\tilde{E}(k) = \tilde{\rho}(k), \qquad (3)$$

where $\tilde{}$ represents the Fourier transformed variable in k-space. On inverse Fourier transform (FT^{-1}) we get

$$E(x) = \text{FT}^{-1}\left[\frac{\tilde{\rho}(k)}{ik}\right]. \tag{4}$$

We use FFTW 3.2 for the required Fourier transforms.[20] For large grid sizes in x, as used in this work, error in this method approaches machine precision. We incorporate these algorithms to construct a Vlasov-Poisson solver.

III. SIMULATIONS

In order to simulate Landau damping, following Manfredi,[5] we perturb the distribution function with one mode. Therefore, we initialize the following distribution function:

$$f(x, v, 0) = (1 + \alpha \cos(kx))f_{q_0}(v), \tag{5}$$

where $f_{q_0}(v)$ is the initial q-nonextensive velocity distribution function. The q-nonextensive velocity distribution function[11] is given by

$$f_{q_0}(v) = C_q\left[1 - (q-1)\frac{v^2}{2}\right]^{1/(q-1)}, \tag{6}$$

where q is the strength of nonextensivity and C_q is the normalization constant given by

$$C_q = \begin{cases} \dfrac{\Gamma\left(\dfrac{1}{1-q}\right)}{\Gamma\left(\dfrac{1}{1-q} - \dfrac{1}{2}\right)}\sqrt{\dfrac{1-q}{2\pi}} & \text{for } -1 < q < 1 \\[3em] \left(\dfrac{1+q}{2}\right)\dfrac{\Gamma\left(\dfrac{1}{q-1} + \dfrac{1}{2}\right)}{\Gamma\left(\dfrac{1}{q-1}\right)}\sqrt{\dfrac{q-1}{2\pi}} & \text{for } q > 1, \end{cases} \tag{7}$$

where $\Gamma(n)$ represents the standard gamma function. Also, for $q > 1$, the distribution exhibits a velocity cut-off given by $|v_{\text{cutoff}}| = \sqrt{2/(q-1)}$. For $q = 1$, this distribution reduces to the Maxwellian with $C_1 = 1/\sqrt{2\pi}$.

The independent parameters are the strength of perturbation α, the wave number k, and the nonextensive parameter q. In addition, we also consider the bounce time $\tau = \alpha^{-1/2}$, after which the linear solution breaks down and nonlinear effects become prominent (the bounce time τ is the time in which nonlinear trapping becomes important[2]). Therefore, we have developed a nonlinear Vlasov-Poisson solver in order to study this phenomenon for times $t \gg \tau$.

For the present problem, we use the following parameters: We set $L = 2\pi/k$. Throughout the simulations performed, unless mentioned otherwise, we set the strength of perturbation $\alpha = 0.05$ and $k = 0.4$. For the amplitude considered, the bounce time $\tau \approx 4.47$. We also choose $\Delta t = 0.1$, in accordance to the Shannon theorem.[21] With the independent parameters chosen, we now proceed to benchmark the solver.

A. Benchmarking the Vlasov-Poisson solver for linear Landau damping

In order to benchmark the correctness of our Vlasov-Poisson solver, we have developed a numerical solver for the dispersion relation[22] for linear Landau damping. In the past, analytical solutions for the dispersion relation of linear Landau damping for κ-distributions (where $\kappa = 1/(1-q)$) have been carried out in terms of special functions, by Valentini and D'Agosta.[23] However, these solutions were constructed for linear Landau damping under the weakly damped limit, where $|\gamma/\omega| \ll 1$. As the damping rate increases, we find that analytical solutions relying on this assumption deviate significantly from the observed values. Therefore, we have developed a dispersion relation solver valid for arbitrary values of $|\gamma/\omega|$. We also look at the results of our dispersion relation solver for the weakly damped case and compare it with Valentini and D'Agosta as an additional benchmark.

We solve the Ampere equation instead of the Poisson equation in order to replicate the results obtained previously by Vann.[22] We first linearize the Vlasov-Ampere system of equations by choosing $f(x, v, t) = f_{q_0}(v) + f_1(x, v, t)$ and similarly $E(x, t) = E_0(x) + E_1(x, t)$, where the subscript "0" refers to the unperturbed equilibrium solution and the subscript "1" refers to the perturbed correction. At $t = 0$, we assume that the zeroth order or equilibrium electric field to be zero, i.e., $E_0(x) = 0$. Then, we choose ansatz: $f_1, E_1 \sim \exp i(kx - (\omega + i\gamma)t)$, where we have chosen a general angular frequency $\omega + i\gamma$, where ω and γ are real. Substituting the obtained expression for f_1 from the Vlasov equation to the Maxwell equation results in the following dispersion relation:

$$-\omega - i\gamma = \int_{-\infty}^{+\infty}\frac{v(\partial f_{q_0}/\partial v)}{(kv - \omega) - i\gamma}dv. \tag{8}$$

The real and the imaginary parts can be separated to obtain

$$O(\omega, \gamma) : \int_{-\infty}^{+\infty}\frac{(kv - \omega)v(\partial f_{q_0}/\partial v)}{(kv - \omega)^2 + \gamma^2}dv - \text{Im}(z) - \omega = 0, \tag{9}$$

$$G(\omega, \gamma) : \int_{-\infty}^{+\infty}\frac{\gamma v(\partial f_{q_0}/\partial v)}{(kv - \omega)^2 + \gamma^2}dv + \text{Re}(z) - \gamma = 0, \tag{10}$$

where

$$z = \begin{cases} 0 & \text{for } \gamma > 0 \\[1em] 2\pi\left(v\dfrac{\partial f_{q_0}}{\partial v}\right)_{v=v_{\phi i}} & \text{for } \gamma < 0 \end{cases} \tag{11}$$

and where the complex phase velocity $v_{\phi i}$ is given by $kv_{\phi i} = \omega + i\gamma$. We numerically solve both $O(\omega, \gamma)$ and $G(\omega, \gamma)$ simultaneously to arrive at the analytical value of ω and γ to required tolerance.[22]

For a given initial equilibrium distribution function $f_{q_0}(v)$ and a value of k, a domain for ω and γ is chosen. These domains are divided into, say, N, equally spaced parts,

thus creating N^2 cells on the (ω, γ) grid. Then, the values of LHS of $O(\omega)$ and $G(\gamma)$ are calculated over each point on the (ω, γ) grid. The solution lies in cell in which the curve for the zeroes for $O(\omega, \gamma)$ and $G(\omega, \gamma)$ intersect. For this purpose, it is required to search for cells for which both the LHS of $O(\omega, \gamma)$ and $G(\omega, \gamma)$ have different signs on the corners of the cell. Once such a zone has been obtained, it is further divided into N^2 cells, and the procedure is repeated in order to get the solution with better precision. In order to ensure that the solution is detected, one has to choose a large value of N, say, $N = 100$. Also, to reduce the number of cells which satisfy the criteria, but do not contain the solution, we also test for the zeroes of $(O + G)(\omega, \gamma)$ and $(O - G)(\omega, \gamma)$ in addition to the zeros of $O(\omega, \gamma)$ and $G(\omega, \gamma)$. Also, we choose the maximum and minimum values for the domains for ω, γ by ensuring that these limits contain ω, γ calculated from the results of the corresponding simulation.

The solver for linear Landau damping provides us with a precise value for the angular frequency ω and, consequently, the real phase velocity $v_\phi = \omega/k$ and damping rate γ for arbitrary $|\gamma/\omega|$. Also, this solver works for an arbitrary values of k, q, and hence an arbitrary initial q-distribution f_{q_0}. This helps us benchmark the Vlasov-Poisson solver for linear Landau damping, for arbitrary values of ω, k, for arbitrary q-values. From here on, we refer to solutions obtained from numerically solving the dispersion relation (8) as "analytically" obtained value.

We now benchmark the nonlinear Vlasov-Poisson solver using the "analytical" solver for a short period of $t = 200$. For this purpose, we run our simulations for values of q from 0.5 to 1.2. We also have used the analytical solver to compute the values of ω and γ for these runs. We calculate the values of ω and γ from the data obtained from the simulations. ω is calculated from the data for E_1 till $t = 200$ and γ is calculated till the linear phase of Landau damping which lasts till about $t = 25$. Since nonlinear behavior sets in soon after $t \sim 25$, measuring ω till $t = 200$ takes into account the nonlinear oscillations also. This leads to a small discrepancy in ω values between the "analytically" obtained and the observed results. Even so, the observed values are within 3% of the analytical value. The plot for comparison of analytically obtained and observed values of γ can be found in the Fig. 1. We can see that the analytically obtained and values of γ
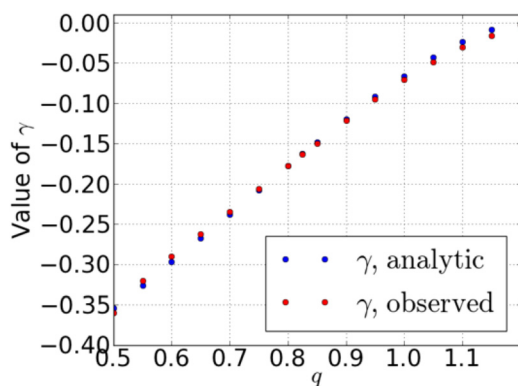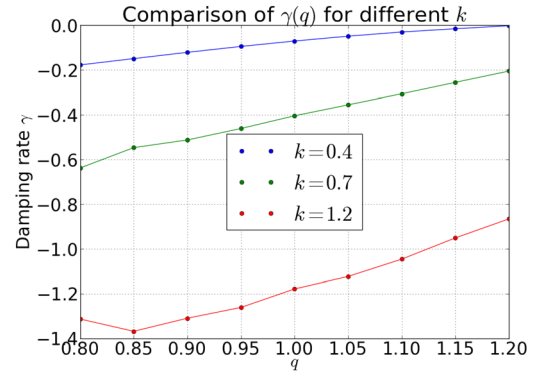

FIG. 2. Plot of damping rate γ as a function of q for values of $k = 0.4, 0.7, 1.2$. One can see that as k increases, the values of $|\gamma|$ are higher than those for a lower k.

obtained during the linear phase of the nonlinear solution match well, demonstrating the correctness of the numerical solver. Also, for $q > 1.2$, the damping rate γ is analytically obtained to be zero, and the corresponding value of ω is such that $v_\phi > v_{\text{cutoff}}$, and hence is unphysical. Also, for $q = 1.2$, even though $v_\phi < v_{\text{cutoff}}$, the phase velocity lies very close to the cut-off velocity. Therefore, the PBC applied on the velocity domain might result in unphysical effects. Hence, we do not consider cases for $q \geq 1.2$. However, for $q = 1.15$, when changing k from 0.4 to 1.2, for $\alpha = 0.05$, the value of $v_\phi = \omega/k$ decreases to lie within the "bulk" of the q-distribution, which enables us to calculate γ accurately. However, on increasing k, the value of the damping rate γ also increases. This can be seen in Fig. 2 for the numerically obtained values of γ varying with q for different k within the linear domain. One can see that the values of $|\gamma|$ for a higher k are larger than those with a lower k. Thus, in general for any value of q, we find that increasing k results in a higher damping rate. This observation has great impact in formation of nonlinear structures. We shall come back to this point later.

As discussed earlier, we have performed an additional benchmark. For example, for sufficiently lower values of k where $|\gamma/\omega| \ll 1$, we have compared our analytical solver with the solution given by Valentini and D'Agosta. We find that for $q = 0.95$ and $k = 0.01$, the analytically obtained value of ω from our dispersion relation solver matches with the result from Valentini and D'Agosta's to 0.016%. Also, among all simulations reported in the present work, the maximum change in energy is observed to be within 0.012%. Now that we are confident about the accuracy of the solver, we proceed to extend the simulations into the long-time regime.

B. Nonlinear Landau damping

1. Case q = 1

Let us consider the simulation for the $q = 1$ case, which is the normalized Maxwellian. For the value of $k = 0.4$, this simulation corresponds to Manfredi's case.[5] Also, we choose N_x and N_v in such a manner that there is sufficient resolution in x and v. Also, a large value of N_v is needed to push the recurrence as far away as possible, which occurs at $T_R = L/\Delta v$. We now proceed to show that we have been able to replicate Manfredi's results with our solver.
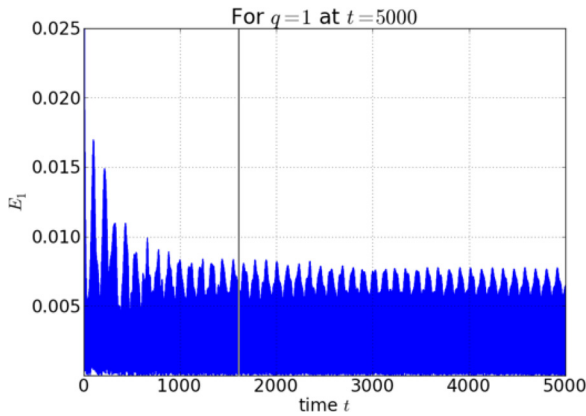

FIG. 1. Comparison of the "analytically" obtained and simulated values of the damping rate γ varying with q ($k = 0.4$, $\alpha = 0.05$).

FIG. 3. A run corresponding to Run I of Manfredi,[5] who had shown the oscillations to continue till $t = 1600$. We extended the run till $t = 5000$. The vertical grey line indicates the duration of Manfredi's simulations. Notice the continuation of the oscillations.

Following Manfredi, the gridsize is set to $N_x = 512$, $N_v = 4000$, which has been shown to be quite accurate for long-time simulations.[5] The choice of parameter results in the recurrence time $T_R \sim 5326$. Also, in the past, BGK structures were seen to be sustained till $t = 1600$.[5] We have extended Manfredi's run till $t = 5000$ and find the electric field structure to sustain. This can be seen in Fig. 3, where we have plotted the amplitude of the fundamental harmonic of the electric field, denoted by E_1, evolving with time. The vertical grey line indicates the duration of Manfredi's simulations.

In the phase-space, a vortex structure is created by particle dynamics during nonlinear evolution. The resonant region is the region in phase-space where phase velocity v_ϕ matches with the particle velocity facilitating resonant exchange of energy between the wave and the particles leading to trapping-detrapping dynamics. Therefore, we look for the vortex in the distribution function f around the phase velocity $v_\phi = \omega/k$ obtained by solving Eqs. (9) and (10) (around which particles exchange energy with the wave). In this case, the analytical value of $\omega = 1.28506$ for $k = 0.4$, and hence $v_\phi = \omega/k = 1.28506/0.4 \approx 3.21$. The plot for phase-space vortex is a frame moving with velocity $v = 3.21$, shown in Fig. 4(a) at time $t = 5000$.

One can see from this figure that there is a phase-space vortex in the distribution function. This, and the figure for E_1, implies that there is a prominent potential well formed, and particles keep getting trapped and detrapped to sustain the steady-state potential well. We can see that this process continues till $t = 5000$, far beyond Manfredi's run of $t = 1600$, demonstrating clearly that such trapping oscillations are sustained for long-time. We now would like to check the velocity distribution function $\hat{f}(v)$ for non-monotonicity generated by nonlinear Landau damping, at $t = 5000$. The velocity distribution function is given by

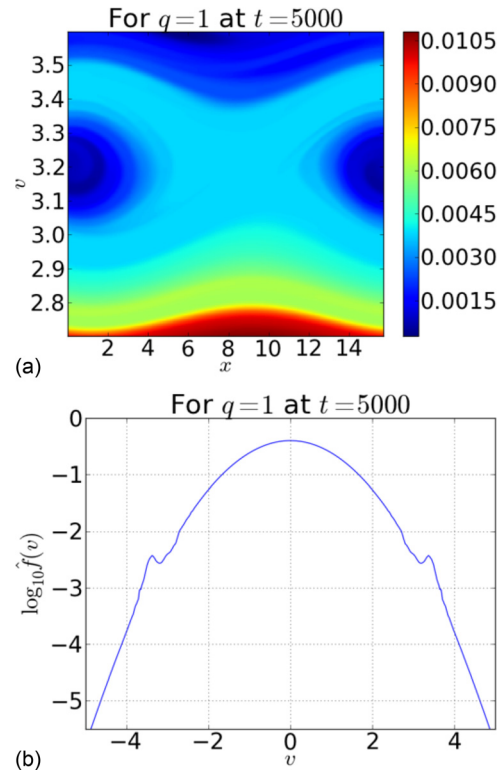$$\hat{f}(v,t) = \frac{\int_0^L f(x,v,t)dx}{\int_{-v_{\max}}^{v_{\max}} \int_0^L f(x,v,t)dxdv}. \tag{12}$$

FIG. 4. For q = 1, at $t = 5000$, the phase-space vortex can be seen around at $v = 3.21$.

In Fig. 4(b), we show the resultant nonmonotonous steady-state velocity distribution function. Existence of phase-space vortex in the frame moving with the phase velocity $v_\phi = \pm 3.21$ is clearly demonstrated. We can also infer that the non-monotonicity of $\log_{10} \hat{f}(v)$ plot can be used to assess the final form of a steady-state travelling wave solution.

In the original work, BGK solutions are constructed by "arranging" number of particles trapped (and untrapped) in potential-energy troughs (and crests), leading to vortices in phase-space and nonmonotonicity in $f(v)$.[3] In our simulations, we observe phase-space vortex structures and its sustenance throughout the time of the simulation. Moreover, this BGK-like structure moves with a constant velocity which accurately matches with the phase-velocity analytically obtained. We, hereon, refer to such solutions as "BGK structures," which, we believe based on the above said arguments, are close to analytically constructed steady BGK modes.

We study the numerical entropy for $q = 1$. The numerical entropy $S(t)$ is computed by

$$S(t) = \int_0^L \int_{-v_{\max}}^{+v_{\max}} f(x,v,t)\log f(x,v,t) \, dv \, dx. \tag{13}$$

We plot relative entropy, defined as $S_{rel} = (S(t) - S(0))/S(0)$, with time. This can be seen in Fig. 5.

Because of the numerical scheme, the entropy monotonically increases with time. The numerical entropy is a measure of the information "lost" from the simulation. As is well known, the evolving distribution function exhibits filamentation which generates a small-scale structure in phase-space. The numerical entropy saturates when the small-scale
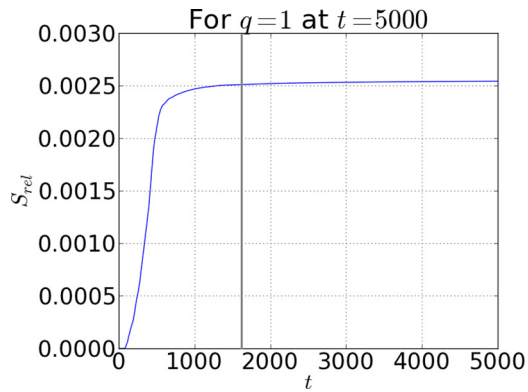
FIG. 5. Plot of relative entropy S_{rel} with time. The vertical line represents the duration of Manfredi's simulation.

structures generated are dissipated when this filamentation reaches the gridsize,[24] rendering a numerical steady-state (nevertheless, the growth of entropy is small, signifying that the information loss is small). Obviously, one can see that the entropy has saturated at around $t = 1500$. It has been shown in the past that such dissipation of small-scale structures do not affect the large-scale solution obtained.[5,24] Also, one can notice that the numerical entropy saturates nearly at the same time the value of E_1 reaches steady-state. Saturation of this numerical entropy in time may be used as a diagnosis to determine the numerical steady-state of the solution in the nonlinear phase.

To summarize $q = 1$ results, we observe that the electric field E_1 initially undergoes few oscillations and then settles to oscillate around a non-zero value. On inspection of the phase-space, we find the phase-space vortex which leads to nonmonotonicity in the velocity distribution function. Also, we find that the phase-space vortex moves with a constant

velocity for the entire simulation. Also, the numerical entropy (which we use as a measure of whether the system has attained a numerical steady-state) saturates at a constant value. Thus, we can infer that this non-zero electric field structure, in a neutral Vlasov plasma, moving with a constant phase velocity, is a BGK-like solution which we call a "BGK structure."

Now that we have observed nonlinear Landau damping on $q = 1$ distribution leading to BGK structure, we wish to study the long-time fate of similar perturbation on $q \neq 1$ distributions. For this purpose, we perform runs for two different sets of q values.

2. Case $q < 1$

In case of $q < 1$, the distribution functions, as compared to the Maxwellian, exhibit a lower peak and a longer tail. Therefore, we choose the following parameters in the solver to accommodate for these changes.

We give runs for $0.5 \leq q < 1$ varied in steps of 0.05 and will be referred to as "Set I." For Set I, we choose $v_{max} = 12.5$, $N_v = 8000$, $N_x = 512$ and keep rest of the initial conditions same as Manfredi's. For these runs, the recurrence time $T_R \sim 5026$, and thus we choose to run the simulation till $t = 2000$. Also, it is important to note that for any q-distribution in this set, we observe that the phase velocity $v_\phi = \omega/k$ lies well within the bulk of the distribution, far from v_{max}.

Now, similar to the case for $q = 1$, we wish to see the evolution of E_1 with time. The graphs obtained for E_1 are plotted in Fig. 6. We have not shown graphs for $q < 0.80$ because for $q \leq 0.80$, E_1 damps and stays damped. Furthermore, with decreasing value of q, the value of $|\gamma|$ increases, and hence the time in which the system damps decreases. Hence, the lesser the value of q, the faster it damps. Also, the behaviour shown
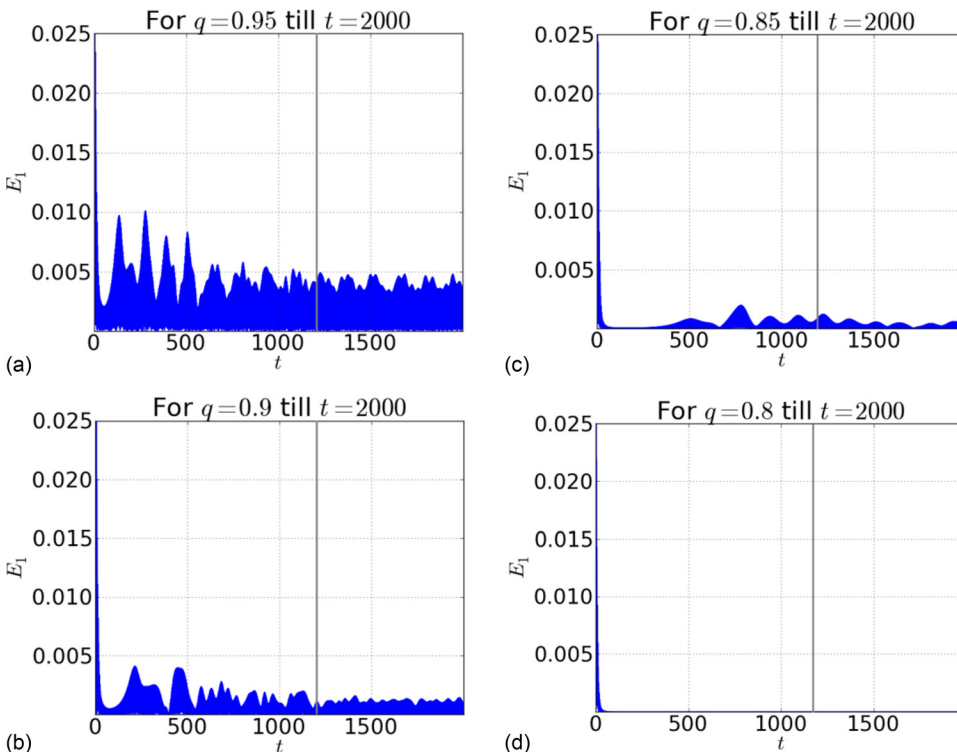

(a)

(b)

(c)

(d)

FIG. 6. Plots for the amplitude of the first harmonic of the electric field E_1 with time for Set I. One can notice that the oscillatory structures are not found for $q \leq 0.80$. Also, as damping rate increases, one can notice that the amplitude of oscillations decreases. This is similar to the result obtained by Valentini.[14] The vertical line represents the time of Valentini's simulations.

by the system is maintained even when the simulation is extended to run till $t = 3000$.

We can see that the oscillations cease to exist somewhere in the interval $q \in [0.80, 0.85]$. We ran the code for an intermediate value of $q = 0.825$. We observe that for this case too the oscillations in E_1 arise, albeit at later time. In fact, we observe that, for those values of q for which BGK structures arise, as q decreases and $|\gamma|$ increases, the time taken for oscillations to arise increases.

Now again, we wish to see the plots for relative entropy with time S_{rel}. In this case, entropy $S(t)$ is defined as[9]

$$S_q(t) = \int_0^L \int_{-v_{\max}}^{+v_{\max}} f(x,v,t) \left(\frac{1 - f(x,v,t)^{q-1}}{q-1} \right) dv\, dx, \quad (14)$$

which is the same as q-nonextensive entropy. Note that for the limit $q = 1$, Eq. (14) reduces to Eq. (13). The plots for relative entropy for Set I can be seen in Fig. 7. For the cases where BGK structures are found, the entropy curves are similar to the curve for $q = 1$. Also, one can notice that smaller the value of q, the later the entropy seems to grow and stabilize. Also, we extended the simulation till $t = 3000$ in order to confirm the formation of a steady-state solution. From the figures for E_1, we conclude that the long-time solution is indeed a BGK structure for $0.85 \leq q \leq 0.95$.

Also, for $q \leq 0.80$, the curves for entropy (not shown) have a different shape, and do not saturate at a fixed value. The phase-space plots of the distribution functions, in the vicinity of v_ϕ, also does not reveal any vortices. For this reason, we believe that within $t = 3000$, cases $q \leq 0.8$ do not lead to phase-space vortices and consequently do not exhibit BGK-like solutions (in order to verify that the monotonic damping for case $q = 0.8$ is not a numerical phenomenon, we ran the same code with higher resolution in x and v, with $N_x = 2048$, $N_v = 16000$, and $v_{\max} = 25$, keeping rest of the parameters the same. For this run too, the oscillations damp quickly and stay damped. Thus, the lack of formation of a BGK structure is not simply a numerical phenomenon).

For the case of $q = 0.85$ (which is close to the value of q for which BGK structures do not form), we wish to see the structure of the distribution function. For $q = 0.85$, the
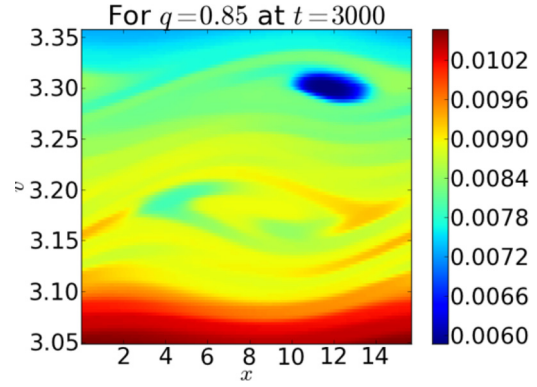
FIG. 8. Plot of distribution function for the run with $q = 0.85$, around $v_\phi = 3.28$, at $t = 3000$.

analytic value of $\omega = 1.31135$ for $k = 0.4$ and, hence, $v_\phi = \omega/k \sim 3.28$. Thus, we plot the distribution function around v_ϕ. The plot can be seen in Fig. 8. Even though, for $q = 0.85$, a phase-space vortex is formed in the vicinity of $v = v_\phi$. This structure is better formed for $q = 0.9$, for which the amplitude of E_1 is greater than that of $q = 0.85$ and thus looks "weak" in the figure, which is similar to the result obtained by Valentini.[14] We can also see that this structure has sustained till $t = 3000$. Thus, from E_1, S_{rel}, and the phase-space vortex, we can conclude that the solution is a BGK structure.

Furthermore, in terms of the independent parameters in the simulation, for $k = 0.4, \alpha = 0.05$, the value of $q \sim 0.8$ seems to be the critical q at which the transition of behavior from completely damped to formation of BGK mode occurs. Therefore, one can say that the window for sustaining BGK modes in $q < 1$ is restricted by the damping rate $|\gamma|$ which increases for decreasing q. Thus, below the critical q, the electric field is damped away before a potential well for trapping is formed.

Now, we move on to the next set of runs corresponding to $q > 1$.

3. Case $q > 1$

We can notice from the velocity distribution function Eq. (7) that for $q > 1$, the distribution function exhibits higher peak and a shorter tail. Also, it exhibits a velocity cutoff at $v_{\text{cutoff}} = \sqrt{2/(q-1)}$, beyond which the function becomes unphysical.

Again, similar to Set I, we give runs for $1 < q \leq 1.15$ in steps of 0.05 and refer to this set of runs as "Set II." For the Set II, we choose $v_{\max} = v_{\text{cutoff}}$ and keep grid sizes and rest of the initial conditions the same. The minimum value for the recurrence time $T_R \sim 9934$ (as a result of smaller $v_{\max}$).

In this case, the periodic boundary conditions (PBCs) set on the v-domain may affect the simulations if the resonant region is close to the boundaries. Therefore, we consider only those cases for which the resonant region is sufficiently far away from the boundaries. Hence, as mentioned earlier, we do not consider cases $q \geq 1.2$, as $v_{\text{cutoff}} \lesssim v_\phi$ for increasing $q > 1$. Clearly, one can increase the value of k so as to make the value of $v_\phi = \omega/k$ lie within the "bulk" of the distribution function. However, as we have
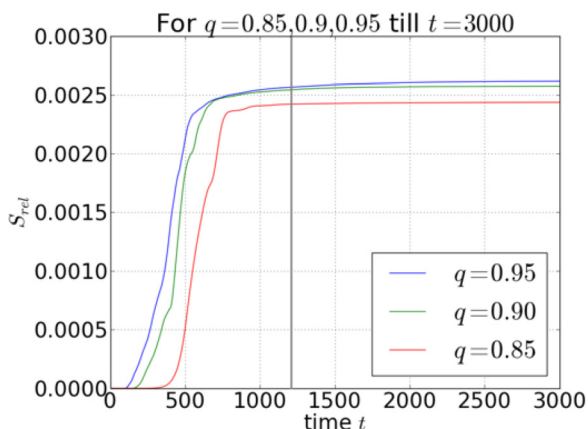

FIG. 7. Plot of relative entropy S_{rel} with time for $q < 1$ till $t = 3000$. The vertical line represents the time up to which Valentini's simulations were performed.

observed, increasing k leads to an increase in γ and, there-fore, the advantage of having v_ϕ more distant from v_{cutoff} is overshadowed by the field being damped rapidly (Fig. 2). We shall come back to this point soon.

For the cases $1.05 \leq q \leq 1.15$, we now wish to see the evolution of E_1 with time. These can be seen in the Fig. 9. One can notice that the oscillations continue at a non-zero amplitude, similar to $q = 1$. Next, we now check $S_{rel}(t)$ to see whether filamentation affects the long-time solutions. This can be seen in Fig. 10. The shape of entropy curves are different from the earlier cases, which may be because of higher resolution in v domain. One can see that the entropy has not saturated within $t = 1200$. However, it can be clearly seen, for $1.05 \leq q \leq 1.15$, that the relative entropy curves settles to steady-state at a higher value than the other q values, within $t = 3000$.

For $q = 1.15$, we wish to see the distribution function at around $v = v_\phi$. In this case, the analytically obtained $\omega = 1.22917$ and, hence, $v_\phi \sim 3.07$. Thus, we plot the
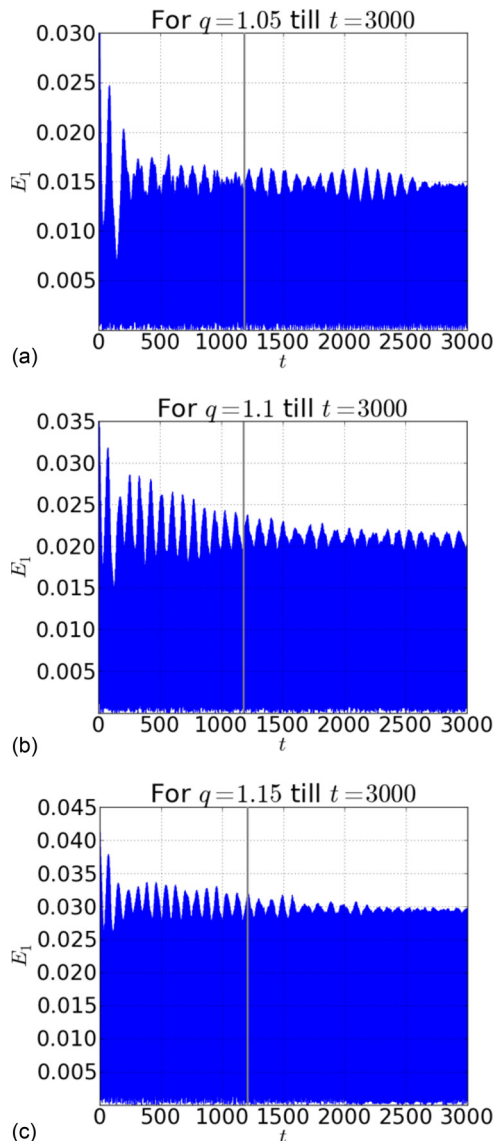

FIG. 10. Plot of relative entropy S_{rel} with time for $1.05 \leq q \leq 1.15$. It can be seen that the entropy saturates within $t = 3000$. The vertical line represents the time up to which Valentini's simulations were performed.

distribution function around v_ϕ at $t \sim 2000$. This can be seen in Fig. 11. In this case too we can see the phase-space vortex clearly and see the corresponding value for E_1, which resembles the case for $q = 0.95$ and $q = 1$. Thus, this long-time state is also a BGK structure solution.

However, for higher q-values, the decrease in v_ϕ is offset by a competing higher k damping. To keep $v_\phi \ll v_{\text{cutoff}}$, k has to be increased. For this purpose, we perturb with a higher value of k, initialized with $q = 1.30$ distribution. We keep α and the grid sizes same as in the earlier cases. Increasing k causes the value of v_ϕ to decrease. We perturb with $k = 0.7$, 1.2, which corresponds to $v_\phi \sim 2.29, 2.07$, respectively, both under $v_{\text{cutoff}} \sim 2.58$. On perturbing with $k = 0.7$, we see oscillations in E_1 (implying a BGK mode solution) and perturbing with $k = 1.2$, we see that E_1 gets damped quickly and stays damped. This occurs because, with increasing k, keeping α constant, as mentioned earlier, the absolute value of γ increases (Fig. 2), which renders difficult the formation of BGK structures. For Maxwellian plasma, this effect has been observed in the past.[24] Therefore, we may reasonably expect such a transition for any q-distribution which shows BGK structures for some value of α, k. This phenomenon was not considered by Valentini, who states that trapping for $q > 1$ is extremely efficient.[14] We, however, find that the efficiency of

FIG. 9. Plots for the amplitude of the first harmonic of the electric field E_1 with time. The vertical line represents the time of Valentini's simulations. As we can see, the field has not saturated within this time.
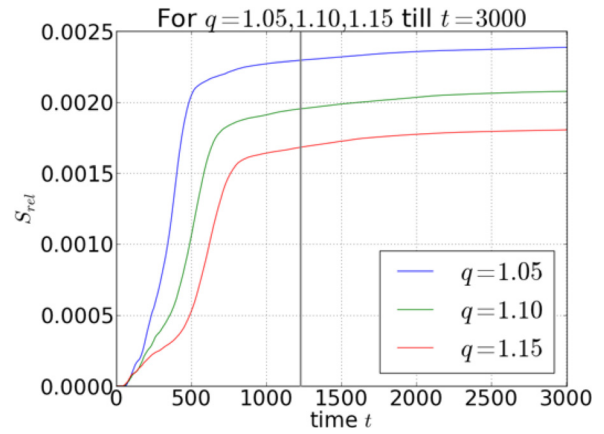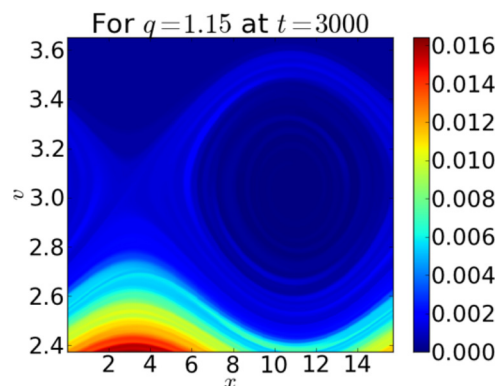

FIG. 11. Plot of distribution function for the run with $q = 1.15$, around $v_\phi = 3.07$, at $t = 3000$.

trapping decreases with increasing k, eventually leading to monotonic damping at a critical k.

As discussed before, the change in behaviour from trapping to monotonic damping is also known to occur for Maxwellian ($q = 1$). In order to check, we gave runs for $q = 1$ with $k = 0.4$–1.2, with the same α, till $t = 2000$. We found that the critical value of k lies between 0.49 and 0.5, between which the behaviour changes from BGK mode formation to exponential damping. For $q = 1$, for this critical value of k, for $\alpha = 0.05$, we find that $\gamma\tau \sim 0.67$. As pointed out empirically by Manfredi, the index $\gamma\tau$ plays a critical role in determining the long-time behaviour of the system. For an initial Maxwellian, it has been previously reported by Manfredi that there seems to be a critical value of $\gamma\tau \sim 0.5$ around which the behaviour of a system changes.[5] However, Ivanov et al. have reported a critical $\gamma\tau \sim 1$ for such a change.[7] Valentini has subsequently studied the dependence of critical value of τ on q for q-distributions.[14] Furthermore, for another value of $k = 0.5$, we have studied the variation in the value of $\gamma\tau$ for different values of q in the linear phase of Landau damping. We observe that for $q \leq 0.9$, $\gamma\tau > 1$. Since we have already seen that $k = 0.5$, $q = 1$ represents a critical value of the change in behaviour and that the damping rate increases with decreasing q, we can reasonably conclude that trapping is not observed for those q-values for which $\gamma\tau > 1$. It is also reasonable to generalize that damping at k values higher than a critical value occurs for any q-distribution. Especially for q-distributions with $q > 1$, this phenomenon severely restricts the window in k within which one can observe BGK modes. Now, we wish to compare the results obtained from the runs corresponding to $0.85 \leq q \leq 1.15$, for which a BGK mode solutions are formed. To do so, we construct a semi-log plot for the velocity distribution function $\hat{f}(v)$ to see where the phase-space vortex is. This can be seen in Fig. 12. For these values of q, from Fig. 12, one can notice that distinct non-monotonicity is observed the vicinity of $v = \pm v_\phi$. Also, for the case of $q = 0.85$, for which the field E_1 is weak, we can see that this structure looks rather diminished. Also, this non-monotonicity becomes more prominent and visible with increasing q. Thus, one can say that BGK structures, for a given perturbation, can occur beyond the critical value of q as

long as v_{cutoff} is greater than and sufficiently far away from v_ϕ. Also, as q increases higher damping rate at larger k values severely limits the window in q for the formation of steady-state BGK structures.

IV. SUMMARY

For a given perturbation amplitude α and perturbation wavenumber k, we demonstrate existence of a window in q where BGK structures are shown to sustain for very long times. For example, for $k = 0.4$, $\alpha = 0.05$, there is a window around $q = 1$ for which we can see BGK structures. As q decreases below $q = 1$, the electric field damps quicker. After a critical value of q, damping renders the existence of BGK structures difficult and, hence, the electric field is found to monotonically damp away. Therefore, for $q < 1$, the formation of BGK modes is limited by the increasing damping rate γ with decreasing q and, in the process, confirmed Valentini's observation up to $t = 3000\omega_p^{-1}$.

As q increases beyond $q = 1$, the perturbation causes the phase velocity to come closer to the velocity cutoff of the $q > 1$ distribution. Because of this, there exists an upper limit on q below which we find BGK structures. Beyond this limit, the perturbation does not cause Landau damping (hence rendering such a situation unphysical). To remedy this, we increased the value of k, which causes the phase velocity to lie within the bulk of the distribution. But, this also causes the damping rate to increase, and, thus, a critical value of k exists beyond which BGK structures cannot be found. Thus, in the $q > 1$ domain, whenever nonlinear Landau damping occurs, the formation of BGK structures is limited by an upper limit on k. This had not been observed previously and leads to a severe restriction on the window for $q > 1$ within which trapping occurs.

We have shown, using high-resolution Vlasov-Poisson solver for long-times up to $t = 3000\omega_p^{-1}$ that the formation of BGK structures seems to depend critically on the independent parameters q, k, α. Further work needs to be done to explore the dependence of formation of BGK structures on the independent parameters of the simulation, which will be reported in a future publication.
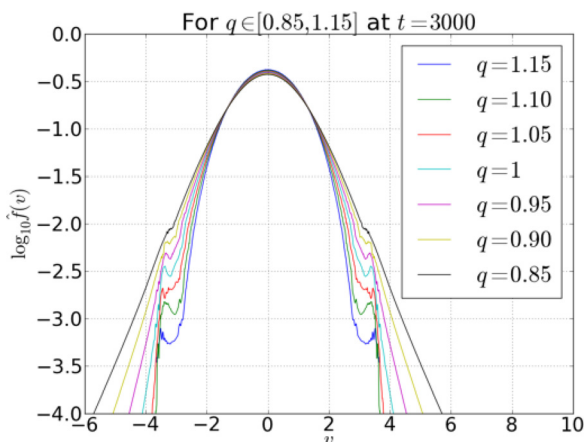
FIG. 12. Plot of velocity distribution function $\log_{10}\hat{f}(v)$ at $t = 3000$ comparing cases with $0.85 \leq q \leq 1.15$.

[1]L. Landau, J. Phys. USSR **10**, 25 (1946) [English translation reproduced in Collected papers of L.D. Landau, edited by D. ter Haar (Pergamon, 1965), pp. 445–460].
[2]T. O'Neil, Phys. Fluids **8**, 2255 (1965).
[3]I. B. Bernstein, J. M. Greene, and M. D. Kruskal, Phys. Rev. **108**, 546 (1957).
[4]M. B. Isichenko, Phys. Rev. Lett. **78**, 2369 (1997).
[5]G. Manfredi, Phys. Rev. Lett. **79**, 2815 (1997).
[6]M. C. Firpo and Y. Elskens, Phys. Rev. Lett. **84**, 3318 (2000).
[7]A. Ivanov, I. Cairns, and P. Robinson, Phys. Plasmas **11**, 4649 (2004).
[8]J. Barré and Y. Y. Yamaguchi, Phys. Rev. E **79**, 036208 (2009).
[9]C. Tsallis, J. Stat. Phys. **52**, 479 (1988).

[10]R. Silva, Jr., A. R. Plastino, and J. A. S. Lima, Phys. Lett. A **249**, 401 (1998).

[11]M. Tribeche, L. Djebarni, and R. Amour, Phys. Plasmas **17**, 042114 (2010).

[12]A. Lavagno and P. Quarati, in Proceedings of the Sixth International Workshop on Topics in Astroparticle and Underground Physics [Nucl. Phys. B 87(Suppl.), 209 (2000)].

[13]A. Lavagno, G. Kaniadakis, M. Rego-Monteiro, P. Quarati, and C. Tsallis, Astrophys. Lett. Commun. **35**, 449 (1998).

[14]F. Valentini, Phys. Plasmas **12**, 072106 (2005).

[15]C. Z. Cheng and G. Knorr, J. Comput. Phys. **22**, 330 (1976).

[16]T. Arber and R. Vann, J. Comput. Phys. **180**, 339 (2002).

[17]E. Fijalkow, Comput. Phys. Commun. **116**, 319 (1999).

[18]P. Colella and P. R. Woodward, J. Comput. Phys. **54**, 174 (1984).

[19]J. P. Boris and D. L. Book, J. Comput. Phys. **11**, 38 (1973).

[20]M. Frigo and S. G. Johnson, Proc. IEEE **93**, 216 (2005).

[21]A. Ghizzo, B. Izrar, P. Bertrand, E. Fijalkow, M. R. Feix *et al*., Phys. Fluids **31**, 72 (1988).

[22]R. Vann, "Characterisation of fully nonlinear Berk-Breizman phenomenonology," Ph.D. dissertation (University of Warwick, 2002).

[23]F. Valentini and R. D'Agosta, Phys. Plasmas **14**, 092111 (2007).

[24]M. R. Feix, P. Bertrand, and A. Ghizzo, in *Advances in Kinetic Theory and Computing*, edited by B. Perthame (World Scientific, Singapore, 1994), pp. 45–81.